Stent Shape Estimation through a Comprehensive Interpretation of Intravascular Ultrasound Images*

Francesco Ciompi[1,2], Simone Balocco[1,2], Carles Caus[3], Josepa Mauri[3], and Petia Radeva[1,2]

[1] Dep. of Applied Mathematics and Analysis, University of Barcelona, Spain
[2] Computer Vision Center, Campus UAB, Bellaterra, Barcelona, Spain
[3] Hospital Universitari "Germans Trias i Pujol", Badalona, Spain
fciompi@cvc.uab.es

Abstract. We present a method for automatic struts detection and stent shape estimation in cross-sectional intravascular ultrasound images. A stent shape is first estimated through a comprehensive interpretation of the vessel morphology, performed using a supervised context-aware multi-class classification scheme. Then, the successive strut identification exploits both local appearance and the defined stent shape. The method is tested on 589 images obtained from 80 patients, achieving a F-measure of 74.1% and an averaged distance between manual and automatic struts of 0.10 *mm*.

Keywords: IVUS, Stent detection, Stacked Sequential Learning.

1 Introduction

An intraluminal coronary stent is a metal mesh tube deployed in a stenotic artery during Percutaneous Coronary Intervention (PCI), in order to prevent the vessel narrowing after balloon angioplasty. After stent placement, cases of underexpansion (stent correctly placed but not completely expanded) or malaposition (stent only partially in contact with the luminal wall) may be experienced. These cases are recognized as important risk factors and might lead to restenosis [1]. In both cases, the definition of the stent shape, compared with the luminal border and the vessel border, allows to assess the stent placement in the vessel.

The appearance of struts can be obtained by Intravascular Ultrasound (IVUS), a catheter based imaging technique that provides the sequence of tomographic images (pullback) of the internal vessel morphology. The appearance of a stent in IVUS is shown in Figure 1(a), which represents a cross-section of the artery.

The condition of stent placement in the vessel can be deduced by the position of its structural elements (*struts*), (see Figure 1(a,b)). Unfortunately, often only a few struts are visible in the IVUS image, due to the inclination of the ultrasonic probe with respect to the longitudinal axis of the vessel and to the presence of calcification or a dense fibrosis in contact with the stent. On the other hand,

* This work was supported in part by the MICINN Grants TIN2009-14404-C02.

K. Mori et al. (Eds.): MICCAI 2013, Part II, LNCS 8150, pp. 345–352, 2013.

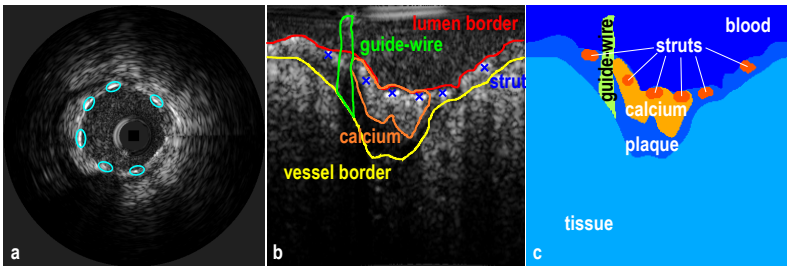

Fig. 1. Example of IVUS image in short-axis (a) and polar form (b). In (a), stent struts are marked; in (b), manual contours of main vessel areas are indicated. In (c), the map of classes obtained by processing the annotations in (b) is depicted.

several regions in the IVUS image may be confused with a strut, due to their local appearance. Clear examples are artifacts produced by the guide-wire, refractions of ultrasonic waves, reverberations, or presence of small calcifications.

Despite the importance of stent analysis in clinical practice, the problem of modeling a stent shape and detecting struts was solely tackled in [2,3,4,5,6], and never in a unique framework. Regarding stent modeling in [2], two deformable cylinders corresponding to the luminal wall and the stent were used. The cylinders were adapted to image edges and ridges to obtain a three-dimensional reconstruction of the boundaries. A semi-automatic stent contour detection algorithm was presented in [3]. The method performs a global modeling of struts by minimum cost algorithm, followed by refinement using local information on stent shape and image intensity gradient. User interaction is finally foreseen to correct the stent shape in 3D. In [4], the same authors proposed an improved version of this method, where the stent shape is accurately reconstructed in images with good quality, but the algorithm requires at least three clearly visible struts.

The problem of struts detection was instead tackled in [5,6]. An automatic method, limited to bio-absorbable stents, was proposed in [5], using Haar-like features and a cascade of classifiers. Recently, a detection algorithm based on two-stage classification for fully automatic stent detection, has been presented [6]. Despite the encouraging results, the number of false positive struts makes the method not suitable for clinical purposes.

Our Contribution. We present a novel methodology that jointly formulates (1) automatic stent shape estimation and (2) struts detection. Differently from previous methods, in our approach the struts detection is constrained by the stent shape assessment. The overall layout of the methodology is depicted in Figure 2. The idea is that the stent shape can be approximated by considering both (a) presence of struts and (b) vessel morphology, which partially solves the problem of lack of visible struts. A curve is first estimated through a comprehensive interpretation of the vessel morphology. For this purpose, morphologic regions in the vessel are modeled using the context-aware classification framework presented in [7], where the class *strut* is added. Successively, the struts are detected

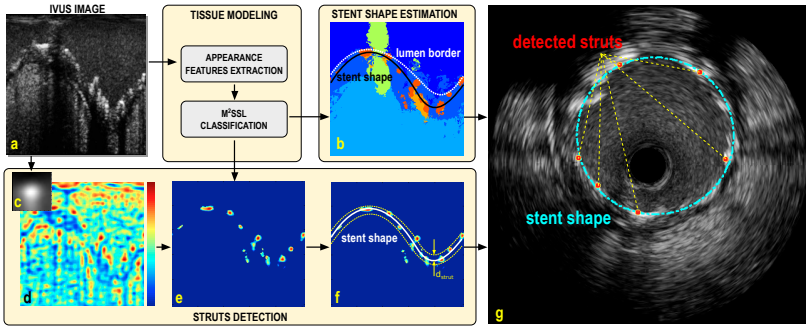

Fig. 2. Schematic representation of the framework. The IVUS image (a) is the input, (b) is the map of classified regions, with the estimated stent shape. The estimated strut kernel (c) allows to compute the struts likelihood map (d) that, combined with classified struts (e) and with the stent shape (b), is used to identify the struts centers (f). In (g) the detection result in short-axis is depicted.

based on both local *appearance* and stent model, which allows a reduction of false positives detection. To the best of our knowledge, this is the first time that both stent shape and struts position are jointly identified in a fully automatic framework. The method is formulated without making any assumption on stent type and imaging parameters and validated with a highly heterogenous dataset of 589 IVUS images from 80 in-vivo arteries.

2 Method

Classification. A multi-class classifiers is used to identify the main morphologic regions in the IVUS image. For this purpose, six regions are defined by manual annotation: *blood (B), plaque (P), calcium (C), guide-wire (G), strut (S), tissue (T)* (see Figure 1 (b,c)). For classification purposes, we adopt Multi-Scale Multi-Class Stacked Sequential Learning (M^2SSL), which has been shown to provide a robust interpretation of the IVUS image [7].

The M^2SSL is a classification architecture based on two *stacked* classifiers, namely H_1 and H_2. The classifier H_1 is fed with a set of features $\mathbf{x}_A$ of tissues *appearance*, computed for each position $\boldsymbol{q} = (\rho, \theta)$ of the IVUS image in polar coordinates, and provides as output a vector $\mathcal{P} \in \mathbb{R}^{1 \times N_c}$ of pseudo-likelihoods, where N_c is the number of classes. As in [7], the ECOC technique is used to deal with multi-class problem, and to compute the vector $\mathcal{P}(\boldsymbol{q})$ for any location of the image. The classifier H_2 is fed with the combination of $\mathbf{x}_A$ with features of *context* $\mathbf{x}_C$. The role of $\mathbf{x}_C$ is to encode long-range interactions between regions in the image. This is done through a multi-scale sampling of the map $\mathcal{P}$ at N_s scales. At each scale s, the map is smoothed with a Gaussian kernel of standard deviation $\sigma_s = 2^{(s-1)}$ and then sampled in positions corresponding to the 8N neighborhood of each location $\boldsymbol{q}$ for each class. The central pixel is included as well: as a consequence, $|\mathbf{x}_C| = 9N_cN_s$. Finally, an *extended* feature vector $\mathbf{x}_E = [\mathbf{x}_A\ \mathbf{x}_C]$ is provided to H_2, which assigns the label Y pixel-wise.

Features of Appearance, $\mathbf{x}_A$. The features of appearance in IVUS are obtained by joining 30 textural descriptors. First, from the set of features in [7], we select a subset of operators: Gabor filters, Local Binary Patterns, and the shadow-related features. Then, we introduce two novel operators that are specific for the strut detection problem. The first one is related to the oval-like strut appearance in images and is defined as $I_{BD} = -I * L_\gamma$, where L_γ is the Laplacian of Gaussian with parameter γ and I is the IVUS image. We apply the filter for values $\gamma = \{2, 3, 4, 5, 6\}$, and for each position $\boldsymbol{q}$ we consider the feature vector $\mathbf{x}^{\boldsymbol{q}}_{BD} = [I^{\boldsymbol{q}}_{BD}|_{\gamma=2}, \ldots, I^{\boldsymbol{q}}_{BD}|_{\gamma=6}] \in \mathbb{R}^{1\times 5}$.

The second operator is related to blood characterization, and consists in the cross-correlation between subsequent images of the pullback. Given a position p_i of one frame in a sequence, we consider three adjacent frames $\{I_{p_i-1}, I_{p_i}, I_{p_i+1}\}$, and we apply cross-correlation $\mathcal{R}$ between squared sliding windows of size W_{cc} over the three *pairs* of frames $\{(I_{p_i-1}, I_{p_i}), (I_{p_i}, I_{p_i+1}), (I_{p_i-1}, I_{p_i+1})\}$. The feature is assigned to each pixel in position $\boldsymbol{q}$ as $\mathbf{x}^{\boldsymbol{q}}_{CC} = \frac{1}{3}(\mathcal{R}_{p_i,p_{i-1}} + \mathcal{R}_{p_i,p_{i+1}} + \mathcal{R}_{p_{i-1},p_{i+1}})$. We vary the size W_{cc} from 5 to 11 pixel with a step of 2 pixel, obtaining $|\mathbf{x}^{\boldsymbol{q}}_{CC}| = 4$.

Stent Shape Estimation. Estimating the stent shape consists in finding a curve that simultaneously fulfills three criteria: (1) the shape should cross as many struts as possible; (2) it should fulfill morphologic constraints with respect to the vessel structure (e.g., no struts inside a calcified region); (3) given the rigidity of the stent meshes, the shape should be as regular as possible.

Considering (3), we assume the *ellipsis* as a model for the stent shape, which has more degrees of freedom than the circular shape used in [4]. In polar coordinates, the ellipsis is expressed as $\rho(\theta) = \frac{P(\theta)+Q(\theta)}{R(\theta)}$, where:

$$P(\theta) = \rho_0[(b^2 - a^2)cos(\theta + \theta_0 - 2\phi) + (a^2 + b^2)cos(\theta - \theta_0))],$$

$$Q(\theta) = \sqrt{2}ab\sqrt{R(\theta) - 2\rho_0^2 sin^2(\theta - \theta_0)},$$

$$R(\theta) = (b^2 - a^2)cos(2\theta - 2\phi) + a^2 + b^2.$$

The curve is thus defined by the set of parameters $\mathcal{E} = [a, b, \phi, \rho_0, \theta_0]$, indicating, in order, the major (a) and minor (b) axes, the orientation (ϕ) and the coordinates (ρ_0, θ_0) of the center of the ellipsis.

Following criteria (1,2), a robust estimation of stent shape is obtained through a comprehensive interpretation of the curve position with respect to the vessel morphology. For this purpose, similarly to [7], we design a functional $\Psi(\mathcal{E})$ that encodes the dependencies between parameters of the stent curve and vessel morphology: $\Psi(\mathcal{E}) = \sum_{i=1}^{|\boldsymbol{t}^+|} w_i t(\mathcal{E})_i^+ - \sum_{j=1}^{|\boldsymbol{t}^-|} w_j t(\mathcal{E})_j^-$. Based on the classification output, $\boldsymbol{t}^+ = \{t(\mathcal{E})_i^+\}$ and $\boldsymbol{t}^- = \{t(\mathcal{E})_j^-\}$ are the regions of the image positively or negatively contributing to the correct curve placement, due the relationship with the vessel morphology. Given the tissue nomenclature, we define $\boldsymbol{t}^+ = \{L_\uparrow, P_\uparrow, C_\downarrow, L_\downarrow, P_\downarrow, C_\curvearrowright, P_\curvearrowright, S_\curvearrowright\}$ and $\boldsymbol{t}^- = \{C_\uparrow, S_\uparrow, T_\uparrow, S_\downarrow,\}$, where the arrows indicate a region placed above ($\uparrow$), below ($\downarrow$) or crossed ($\curvearrowright$) by the

curve. The stent shape is estimated as $\mathcal{E}_{stent} = argmin_{\mathcal{E}}(-\Psi(\mathcal{E}))$, where the set of coordinates of the stent curve $(\boldsymbol{\rho}(\mathcal{E})_{stent}, \boldsymbol{\theta}(\mathcal{E})_{stent})$ in polar coordinates is obtained by a minimization procedure [8]. The shape is initialized with the elliptic approximation of the *luminal* region of the IVUS image, obtained by considering the area of connected pixels labelled as *blood* close to the region occupied by the catheter (see Figure. 2(b)).

Struts Detection. Once the stent shape is estimated, we can automatically detect the positions $S_A = (\rho_A, \theta_A)$ representative for struts by considering three conditions. First, the appearance of a strut is accounted considering a likelihood map $\mathcal{L}_{strut}(\rho, \theta)$ (see Figure 2(d)), obtained through the normalized cross correlation between the IVUS image and a *kernel* K_S, which represents the local strut appearance (Figure 2(c)). This kernel is learned by averaging the intensity of the pixels in a bounding box of side H[1], centered around the labelled struts in the training set. A local maxima of $\mathcal{L}_{strut}$ identifies a potential strut position.

The strut detection is then subject to two additional conditions: (1) S_A must belong to a region classified as strut $\mathcal{Q}_{strut} = \{\boldsymbol{q}\}|_{Y(\boldsymbol{q})=strut}$; (2) S_A must be proximal with respect to the estimated stent shape. The coordinates of struts are then obtained as $(\boldsymbol{\rho}_{strut}, \boldsymbol{\theta}_{strut}) = argmax_{\boldsymbol{\rho},\boldsymbol{\theta}}(\mathcal{L}_{strut}(\boldsymbol{\rho}, \boldsymbol{\theta}) \bigcap \mathcal{Q}_{strut})$, subject to $dist((\boldsymbol{\rho}_{strut}, \boldsymbol{\theta}_{strut}), (\boldsymbol{\rho}_{stent}, \boldsymbol{\theta}_{stent})) \leq d_{strut}$. We assume the value $d_{strut} = 0.2\ mm \simeq 2H$, representing a significant value for stent distance in clinical practice, used for example to assess malaposition.

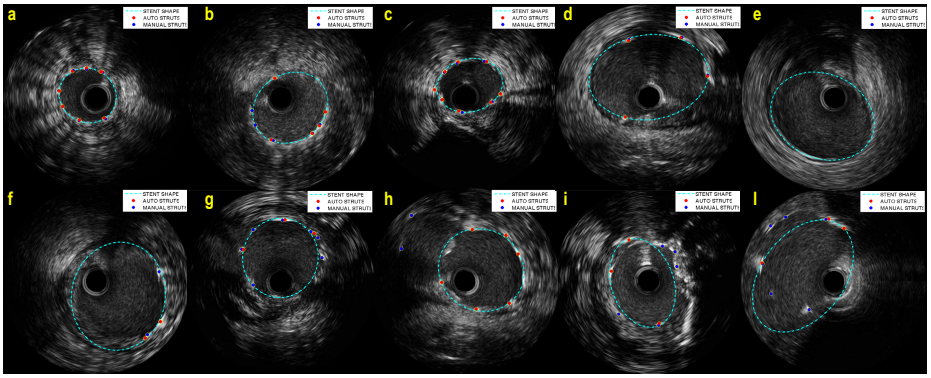

Fig. 3. Examples of stent shape estimation and strut detection. The stent shape is depicted (dotted line) along with the manual annotation (blue circles) and the automatic strut detection (red circles).

[1] The value $H = 0.18\ mm$ was empirically chosen in order to include the strut appearance in the bounding box, along the whole dataset.

Table 1. Quantitative results, where all the frames of TSds are considered (`all`), presence of calcification (`calcium`), bifurcations (`side-branch`), large vessel (`large`), absence of previous cases (`normal`). The mean (`MN`) and median (`MD`) distances between automatic and manual struts (`ss`), and between manual struts and stent curve (`sc`) are indicated. All values are reported in average and (standard deviation).

	`all`	`calcium`	`side-branch`	`large`	`normal`
`Precision` [%]	76.6 (29.2)	70.2 (33.0)	70.4 (33.3)	69.5 (34.4)	77.7 (26.5)
`Recall` [%]	77.5 (30.0)	74.0 (34.4)	68.9 (33.0)	64.9 (32.9)	82.9 (27.2)
`F-measure` [%]	74.1 (26.7)	67.5 (30.2)	66.6 (29.9)	63.6 (29.7)	77.6 (24.1)
`MNss` $[mm]$	0.10 (0.10)	0.10 (0.09)	0.10 (0.10)	0.11 (0.10)	0.09 (0.10)
`MDss` $[mm]$	0.07	0.07	0.08	0.08	0.07
`MNsc` $[mm]$	0.14 (0.22)	0.21 (0.27)	0.22 (0.36)	0.21 (0.29)	0.11 (0.18)
`MDsc` $[mm]$	0.07	0.11	0.09	0.09	0.06

3 Validation

Experimental Setup. A set of 93 IVUS pullbacks of different patients were used in this study. The IVUS sequences were acquired using iLab echograph (Boston Scientific) with a 40 MHz catheter; no standardization of the echograph parameters was applied during the acquisitions. Data acquisition protocol was approved by the ethical committee of the university hospital. For training purposes, 180 frames were randomly extracted from 13 pullbacks, assuring a proportion of 50% between frames with and without stent, representing the dataset $TRds$. In order to train H_1 and H_2 with different data, $TRds$ was split into two balanced subsets $TRds_1$ and $TRds_2$, containing 90 frames each. The remaining 80 pullbacks were used for testing purposes. An expert identified the range of frames containing the stent in each pullback, and 589 frames were randomly selected within this range to create the test set $TSds$. The same expert manually labelled the regions described in section 2 in each selected frame of $TRds$, and manually marked the central position (ρ_M, θ_M) of each visible strut in $TSds$. The areas containing struts in $TRds$ were assigned as a circular shape centered in (ρ_M, θ_M), with a radius of $H/2$. In the M^{2}SSL architecture, the binary classifier for both H_1 and H_2 is Adaptive Boosting, and it is trained with up to 150 decision stumps. The training strategy in the ECOC framework is one-vs-one. The number of scales in M^{2}SSL is $N_s = 6$, covering up to half of the image size. The training of the weights $\mathbf{w} = \{w_i, w_j\}$ is done by approximating manual struts annotations with an ellipsis, and then averaging the normalized amount of tissues over $TRds$ by cross-validation.

Performance Evaluation. The validation of the proposed method includes two evaluations. First, in order to assess the performance of the struts detection, we consider parameters *Precision*, *Recall*, and *F-Measure*. The set of positions of struts manually labelled (ρ_M^i, θ_M^i) and the ones obtained by automatic detection (ρ_A^j, θ_A^j) are used to compute true positives (TP), false positives (FP) and false negatives (FN). The presence of a detected struts (ρ_A^j, θ_A^j) inside a circular

region $\mathcal{N}$ of radius H around each (ρ_M^i, θ_M^i) is considered: if $(\rho_A^j, \theta_A^j) \in \mathcal{N}$, it is considered as a TP; if $(\rho_A^j, \theta_A^j) \notin \mathcal{N}$, as FP; if $\mathcal{N} \bigcap \{\rho_A^j, \theta_A^j\} = \varnothing$, it is a FN.

Secondly, in order to assess the performance of the stent shape estimation, we consider distance measures. Since a manual annotation of the full stent shape is not available, the performance is assessed in terms of both (a) radial distance d_{SC} between the strut points (ρ_M^i, θ_M^i) and the stent curve $(\boldsymbol{\rho}_{stent}, \boldsymbol{\theta}_{stent})$ and (b) radial distance d_{SS} between (ρ_M^i, θ_M^i) and (ρ_A^j, θ_A^j). The validation results are reported in Table 1, where the distance measures are indicated in terms of mean values ($\texttt{MN}_{ss}$, $\texttt{MN}_{sc}$) and median values ($\texttt{MD}_{ss}$, $\texttt{MD}_{sc}$). Furthermore, the results grouped by categories of frames containing calcifications (`calcium`, 22.6% of TSds), side-branches (`side-branch`, 8.3% of TSds), large vessel (`large`, 9.7% of TSds) or none of these cases (`normal`, 65.4% of TSds), are also reported.

The obtained value of F-measure (F = 74.1%) indicates a good capability of the method to correctly detect struts, expressing a low number of FPs (P = 76.6%) and of FNs (R = 77.5%), thereby outperforming methods based on similar approach (F = 71% in [5], F = 66% in [6]). In Figure 3, some examples of stent shape estimation and struts detection are depicted.

4 Discussion

Considering the results in Table 1, we observe that the Recall score decreases in images with large vessel. A similar effect is induced by presence of bifurcations, where two stents are implanted and the detected strut may belong to the second stent. In both cases, the suboptimal shape estimation is induced by the low presence of similar cases in the training set, which hampers the possibilities of the learning process to tune correctly the weights $\mathbf{w}$ for the specific morphology. The presence of calcification also affects the performance, since few small calcifications are still confused with struts. In terms of distance measures, the position of the estimated curve with respect to the manual struts ($\texttt{MN}_{sc}$ and $\texttt{MD}_{sc}$) also reflects the presence of these three challenging image typologies. When considering distances between manual and automatic struts position, a fairly constant error is obtained in both $\texttt{MN}_{sc}$ and $\texttt{MD}_{sc}$. This makes possible to characterize the system performance, for struts detection, regardless of the clinical condition of the vessel. It is also worth to note that the value $\texttt{MN}_{ss}$ is four times smaller than the allowed range $2d_{strut}$ around the curve.

The assumption of elliptic shape for the stent holds in most of the frames in $TSds$ ($\approx 95\%$), while in few cases (4.24 %) the stent estimation is inaccurate due to an irregular shape of the vessel. An example is depicted in Figure 3(i), where a big calcification deforms the luminal area into a non-circular shape. This problem could be overcome by using shape information of adjacent frames in the sequence, where a weaker deformation is present. In case of an IVUS frame containing no strut, as the one illustrated in Figure 3 (e), it is worth noticing that the result of the algorithm is still correct, since the comprehensive interpretation of morphology compensates for the lack of struts. In terms of computation time, the current Matlab prototype code takes 4 seconds on a 2.8GHz dual core processor:

1.2 sec for extraction of $\mathbf{x}_A$, 2.7 seconds for H_1 classification, extraction of $\mathbf{x}_C$ and H_2 classification, and 0.1 seconds for stent shape estimation and struts detection. Since the method processes each frame independently, the whole execution can be parallelized, potentially reaching a frame rate of 15 fps. Finally, it is worth to consider that the presented framework can be easily deployed in the future for ultra-high frequency IVUS systems. This will allow to deal with restenosis phenomenon, since its analysis is currently hampered by the limited frequency in available technology.

5 Conclusion and Future Work

We have presented a method for automatic struts detection and stent shape estimation. The proposed approach does not make any assumption on the stent type or the imaging parameters. It outperforms state-of-the-art strut detection methods, and provides a stent shape estimation without making any assumption on the number of visible struts. The capabilities of evaluating whether a generic frame contains a stent has not been evaluated in this paper, and its quantification is planned as future work. Furthermore, given the stent shape, the combination of lumen and media-adventitia measurements will allow the detection of cases of stent malaposition or under-expansion.

References

1. Yoon, H.J., Hur, S.H.: Optimization of stent deployment by intravascular ultrasound. Korean J. Intern. Med. 27(1), 30–38 (2012)
2. Canero, C., Pujol, O., Radeva, P., Toledo, R., Saludes, J., Gil, D., Villanueva, J., Mauri, J., Garcia, B., Gomez, J.: Optimal stent implantation: three-dimensional evaluation of the mutual position of stent and vessel via intracoronary echocardiography. In: Computers in Cardiology, pp. 261–264 (1999)
3. Dijkstra, J., Koning, G., Tuinenburg, J., Oemrawsingh, P.V., Reiber, J.: Automatic border detection in intravascular iltrasound images for quantitative measurements of the vessel, lumen and stent parameters. Computers in Cardiology 28 (Cat. No.01CH37287) 1230, 25–28 (2001)
4. Dijkstra, J., Koning, G., Tuinenburg, J., Oemrawsingh, P.V., Reiber, J.: Automatic stent border detection in intravascular ultrasound images. In: CARS, pp. 1111–1116 (2003)
5. Rotger, D., Radeva, P., Bruining, N.: Automatic detection of bioabsorbable coronary stents in ivus images using a cascade of classifiers. IEEE Transactions on Information Technology in Biomedicine 14(2), 535–537 (2010)
6. Hua, R., Pujol, O., Ciompi, F., Balocco, S., Alberti, M., Mauri, F., Radeva, P.: Stent strut detection by classifying a wide set of ivus features. In: MICCAI Workshop on Computer Assisted Stenting (2012)
7. Ciompi, F., Pujol, O., Gatta, C., Alberti, M., Balocco, S., Carrillo, X., Mauri-Ferre, J., Radeva, P.: Holimab: A holistic approach for media-adventitia border detection in intravascular ultrasound. In: Medical Image Analysis, vol. 16, pp. 1085–1100 (2012)
8. Lagarias, J.C., Reeds, J.A., Wright, M.H., Wright, P.E.: Convergence Properties of the Nelder-Mead Simplex Method in Low Dimensions. SIAM Journal of Optimization 9(1), 112–147 (1998)